Simultaneous polymerization and adhesion under hypoxia in sickle cell disease

Dimitrios P. Papageorgiou[a,1], Sabia Z. Abidi[a,1], Hung-Yu Chang[b], Xuejin Li[b], Gregory J. Kato[c,d], George E. Karniadakis[b], Subra Suresh[e,2], and Ming Dao[a,2]

[a]Department of Materials Science and Engineering, Massachusetts Institute of Technology, Cambridge, MA 02139; [b]Division of Applied Mathematics, Brown University, Providence, RI 02912; [c]Department of Medicine, Heart, Lung, Blood and Vascular Medicine Institute, University of Pittsburgh School of Medicine, Pittsburgh, PA 15261; [d]Division of Hematology–Oncology, Department of Medicine, University of Pittsburgh School of Medicine, Pittsburgh, PA 15261; and [e]Nanyang Technological University, Singapore 639798

Contributed by Subra Suresh, July 13, 2018 (sent for review May 1, 2018; reviewed by Antoine Jérusalem and Kevin T. Turner)

Polymerization and adhesion, dynamic processes that are hallmarks of sickle cell disease (SCD), have thus far been studied in vitro only separately. Here, we present quantitative results of the simultaneous and synergistic effects of adhesion and polymerization of deoxygenated sickle hemoglobin (HbS) in the human red blood cell (RBC) on the mechanisms underlying vasoocclusive pain crisis. For this purpose, we employ a specially developed hypoxic microfluidic platform, which is capable of inducing sickling and unsickling of RBCs in vitro, to test blood samples from eight patients with SCD. We supplemented these experimental results with detailed molecular-level computational simulations of cytoadherence and biorheology using dissipative particle dynamics. By recourse to image analysis techniques, we characterize sickle RBC maturation stages in the following order of the degree of adhesion susceptibility under hypoxia: sickle reticulocytes in circulation (SRs) → sickle mature erythrocytes (SMEs) → irreversibly sickled cells (ISCs). We show that (*i*) hypoxia significantly enhances sickle RBC adherence; (*ii*) HbS polymerization enhances sickle cell adherence in SRs and SMEs, but not in ISCs; (*iii*) SRs exhibit unique adhesion dynamics where HbS fiber projections growing outward from the cell surface create multiple sites of adhesion; and (*iv*) polymerization stimulates adhesion and vice versa, thereby establishing the bidirectional coupling between the two processes. These findings offer insights into possible mechanistic pathways leading to vasoocclusion crisis. They also elucidate the processes underlying the onset of occlusion that may involve circulating reticulocytes, which are more abundant in hemolytic anemias due to robust compensatory erythropoiesis.

sickle cell adhesion dynamics | dissipative particle dynamics | HbS polymerization | microfluidics | hypoxia

Polymerization of deoxygenated sickle hemoglobin (HbS) is the fundamental component of the complex pathophysiology of sickle cell disease (SCD). This disease has both hemolytic and vasoocclusive components, with the latter closely involving abnormal interactions between sickle red blood cells (RBCs) and the vascular endothelium (1). Unlike healthy RBCs, sickle RBCs inherently adhere to human endothelial cells (2, 3). This abnormal adherence of sickle RBCs with the endothelium can occur even under normoxic conditions and for different RBC shapes (3), and is well documented for various endothelia and flow conditions (4). Adherence of sickle RBCs to the endothelium varies markedly among SCD patients (2, 3, 5), and the RBC/endothelium adhesion could likely serve as one of the most important biomarkers that correlates with the clinical vasoocclusive severity of the patient. To date, no clinically measured RBC biomarkers, such as RBC indices, hemoglobin concentration, proportion of irreversibly sickled cells (ISCs), level of fetal hemoglobin, or reticulocyte count satisfactorily predict the severity of an individual patient's clinical experience (5).

The process of vasoocclusion itself depends on enhanced adhesion of sickle RBCs to endothelium, but the underlying mechanisms are not well understood. Microvascular obstruction appears to be a two-step process, which is dependent on RBC density (6). In the postcapillary venules, vessel narrowing is initiated by sickle RBCs that have the highest propensity for adhesion to the vascular endothelium, namely, low-density, deformable sickle cells (7). This process is then followed by entrapment of the least adherent, more dense, and rigid sickle cells (ISCs and unsickleable dense erythrocytes) leading to further occlusion (4, 6, 8). Other blood components driven by inflammatory stimuli also play a role in vasoocclusion (9–11).

In very low-shear stress flow conditions (typically under 0.01-Pa shear stress, about an order of magnitude lower than normally found in postcapillary flow), RBC adherence is transport controlled. In other words, the time for contact between sickle cells and the endothelium is a more important determinant of adherence than high-affinity receptor–ligand interactions (12). Hypoxia enhances RBC adhesion to both macrovascular and microvascular human endothelial cells, with the adhesive receptor, vascular cell adhesion molecule (VCAM-1), mediating this process (13).

In the present study, we developed an in vitro hypoxic microfluidic RBC adherence assay that mimics in vivo sickle cell adhesion in postcapillary venules (~10–100 μm in diameter). Our specially designed experimental setup involves an oxygen pressure-controlled microfluidic device, described in detail in

Significance

Patients with sickle cell disease (SCD) suffer from painful vasoocclusive crises. Polymerization of sickle hemoglobin (HbS) in RBCs is generally considered a major contributor to such crisis events. Here, we present the simultaneous and synergistic coupling of adhesion and HbS polymerization. We show that the age of RBCs in circulation plays an important role in mediating this synergistic effect on blood rheology and clinical symptoms. In particular, the youngest RBCs exhibit unique adhesion dynamics, whereby polymerized HbS fiber bundles grow from cell surfaces to serve as sites of cytoadherence. Our molecular-level simulations show how the attachment and dissociation of molecular bonds influence adhesion dynamics. These results provide a framework that could elucidate the mechanistic basis of SCD vasoocclusive pain crises.

Author contributions: D.P.P., S.Z.A., S.S., and M.D. designed the experiments; D.P.P. and S.Z.A. performed the experiments and analyzed the data; H.-Y.C., X.L., and G.E.K. designed the simulations; H.-Y.C. and X.L. carried out the simulations; G.J.K. provided clinical samples and suggestions on connections between scientific work and clinical practice; and D.P.P., S.Z.A., H.-Y.C., X.L., G.J.K., G.E.K., S.S., and M.D. wrote the paper.

Reviewers: A.J., University of Oxford; and K.T.T., University of Pennsylvania.

Conflict of interest statement: D.P.P., S.Z.A., M.D., and S.S. have filed a patent based on the work presented in this paper.

[1]D.P.P. and S.Z.A. contributed equally to this work.

[2]To whom correspondence may be addressed. Email: ssuresh@ntu.edu.sg or mingdao@mit.edu.

This article contains supporting information online at www.pnas.org/lookup/suppl/doi:10.1073/pnas.1807405115/-/DCSupplemental.

Published online September 6, 2018.

ref. 14, which we further optimized and adapted for the present adhesion study by functionalizing the device wall with fibronectin (FN) (*SI Appendix*, Fig. S1). FN is associated with sickle reticulocyte (SR) binding via the $\alpha_4\beta_1$ integrin receptor (15), and the incubation of endothelial cells with anti-FN antibody has been shown to significantly decrease intrinsic sickle cell adherence by 40% (12).

Sickle cell adherence appears to predominate in postcapillary venules, where the shear stress near the wall is ∼0.1 Pa (4, 16). Invoking this notion, our microfluidic device was designed to have an equivalent hydraulic diameter D_h of about 30 μm. We vary the shear stress, τ, near the walls within the range of 0.035–0.085 Pa to allow RBC adhesion to the wall, but not detachment. Adherence at microvascular low shear stresses of <0.1 Pa is hypothesized to be an important factor that can act either independently or concurrently with acute events to induce adhesive interactions (12).

We also performed computational simulations of cytoadherence in sickle RBCs using a particle-based stochastic model that accounts for bond formation or dissociation (17, 18). This was introduced in conjunction with dissipative particle dynamics (DPD) that models RBCs, blood plasma, and the functionalized surface. The dynamics of adhesive bond formation and dissociation are described by the reaction rate k_{on} (or k_{off}), which strongly depends on the force F between the cell receptors and the endothelial ligands, representing noncovalent interactions (19). Our model has been validated in a number of independent computational studies (20–22), including investigation of the adhesive behavior of RBCs in *Plasmodium falciparum* malaria (20), and hypoxia-induced alterations in adhesion dynamics of RBCs in SCD (22).

Here, we address the following hitherto-unresolved questions of pathophysiological importance at the single-cell level: Is hypoxia-induced adhesion correlated with differences between sickle cell reticulocytes and more mature erythrocytes? What are the mechanisms involved in each maturation stage, which could affect the cell surface contact area and subsequently the propensity for adhesion during shear flow conditions?

Results

Hypoxia Enhances Sickle Cell Adherence. Normoxic individual sickle cells show pronounced morphological heterogeneity, and this variation is considerable even among the same density fraction of cells. Such sickle cells exhibit even greater variation in adhesion dynamics under hypoxia.

Fig. 1*A* shows a snapshot of adherent sickle RBC cascade after ∼10 min of flow (∼0.05-Pa wall shear stress) on a FN-coated microchannel wall under steady-state hypoxia (2% O_2) in a fixed field of view (FOV) within the microfluidic device. The cells were exposed to hypoxic conditions for ∼2 min before their entry into the FOV. As a result, the majority of cells that entered the FOV had already attained their altered shape under hypoxia. The adherent cell percentage is calculated as the number of adhered RBCs divided by the total number of cells that come in contact with the FN-coated surface during their passage through the FOV, for 10 min of constant flow rate under steady-state hypoxia. The morphological heterogeneity of adherent sickle RBCs in hypoxia is evident (Movie S1).

We categorized sickle cells into the following categories, consistent with the classification from prior literature (23–28) (*SI Appendix*, *Adherent Sickle Cells* and *SI Appendix*, Fig. S2): (*i*) sickle reticulocytes in circulation (SRs), (*ii*) sickle mature erythrocytes (SMEs) of any shape, and (*iii*) ISCs. Using our in vitro adhesion assay, we found that hypoxia enhances sickle cell adhesion compared with normoxia controls, consistent with independent observations (13). The table in Fig. 1*B* shows at least a fourfold increase of adherent cell percentage in hypoxia, in comparison with that in normoxia for the same sample. Three patient samples (Table S1) were tested under comparable shear stress ranges in normoxia versus hypoxia, and we found up to a 13-fold increase in the proportion of adherent cells for one of the samples.

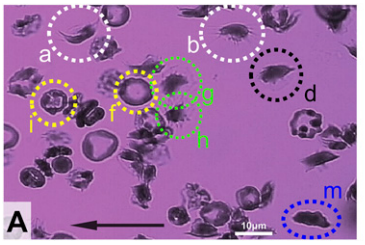

Adherent Cell Percentage		
	Hyp. (%)	Norm. (%)
Patient VI	19.8 ± 6.2	5.0 ± 1.0
Patient VII	44.4 ± 8.9	3.4 ± 1.2
Patient V	53.4 ± 6.9	13.5 ± 4.3

B

Fig. 1. Hypoxia significantly enhances adhesion of sickle RBCs on a FN-coated microchannel wall. (*A*) Morphological heterogeneity of adherent sickle cells under steady-state hypoxia and shear flow in a single FOV over about 10 min. Examples of cell types: (*i*) SRs: a and b (white dotted circles); (*ii*) SMEs: d, g, h, i, and f (green, yellow, and black dotted circles); and (*iii*) ISCs: cell m (blue dotted ellipse). The black arrow denotes the flow direction. Wall shear stress, ∼0.05 Pa. (Scale bar: 10 μm.) Area of FOV, ∼5,766 μm^2 (Movie S1). (*B*) Increase in adherent cell percentage in hypoxia compared with normoxia (see Table S1). The entries here indicate values of mean ± SD.

Studies of cell adhesion alone suggest that heterogeneous cytoadherence among varying cell densities is primarily due to the differences in cell deformability and shape among multiple cell groups, and that it is not influenced by changes in the "adhesion potential" (6, 7). This trend also appears to hold in computational simulations of the adhesion of sickle RBCs with different cell stiffness and morphologies, as in figure 1C in ref. 22, where we compared three sickle cells in terms of adhesion dynamics, with identical adhesion potential and shear flow rate but varying shear moduli (i.e., μ_0, 3 μ_0, and 10 μ_0) and morphology. The mean flow velocity of the RBC with the highest stiffness was consistently higher than the other cells, further validating the hypothesis of heterogeneous RBC adhesive dynamics under shear flow.

Adherence and Polymerization of SMEs. To date, there has been little success in correlating the kinetics of a sickle RBC subpopulation with disease severity (29). While this correlation is key to elucidating SCD pathogenesis, it is also very difficult to validate. To overcome this limitation, we establish correlations of hypoxia-adherent sickle cell classes (as described above) with cell deformability and polymerization kinetics in an attempt to identify a cell population as a potential biomarker that could serve as a predictor of the susceptibility of the patient's cells to adhesion.

In our microfluidic flow device, we subjected human sickle RBCs to normoxia and hypoxia under flow conditions, and observed that SMEs, following initial adhesion to the FN-functionalized surface, could develop more adhesion sites during HbS polymerization. Fig. 2 shows snapshots of SME adhesion dynamics in hypoxia. The cell enters the FOV already "sickled." At the onset of adhesion, the SME develops a pointed membrane edge (white dotted circle in Fig. 2*A*), which attaches to the FN-coated microchannel surface. Immediately thereafter, the cell flips around the main adhesion site to align with the flow direction and transitions from single-site to multiple-site adhesion after ∼2 min of polymerization (Movie S3).

These experiments exhibit the following features:

i) Increase in adhesion sites: Following initial attachment and alignment with the flow, the cell exhibits an oscillatory motion under shear flow, indicative of a single initial adhesion site. After ∼2 min, the oscillation ceases and the cell appears firmly in place, which is a clear indication of the development of multiple adhesion sites.

ii) Polymerized HbS fiber projections: While the cell remains adherent to the FN-coated surface, HbS fibers grow within the cell (black dotted circles in Fig. 2*A*). Those fiber projections ostensibly cause an increase in adhesion sites; their growth appears synchronous with the cessation of cell oscillation (Movie S3).

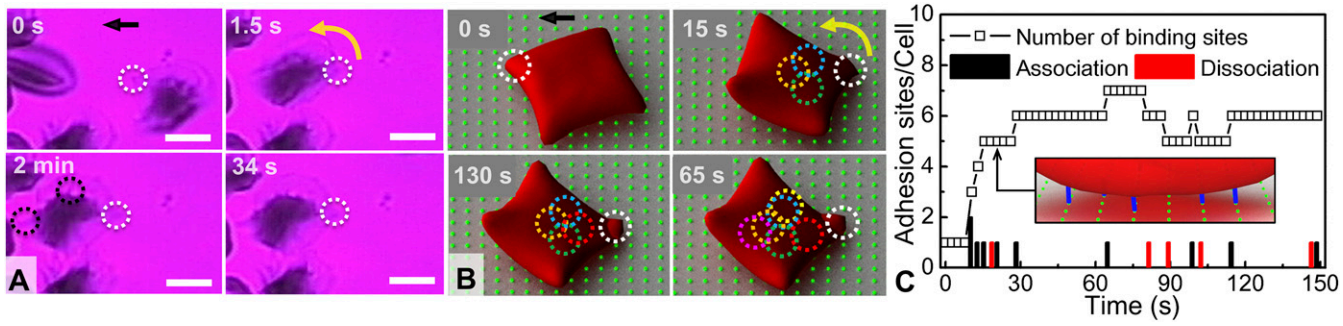

Fig. 2. SME adherence and polymerization: From single-site to multiple-site adhesion. (*A*) Experiment: cell g of Fig. 1*A*. ($t = 0$) The cell adheres on the surface (white dotted circle) while forming a pointed membrane edge (slow-motion Movie S2). (1.5 s < t < 34 s) The cell revolves around the adhesion site and oscillates under flow. ($t = 2$ min) Such oscillatory motion ceases and the cell becomes firmly adherent. The dotted black circles indicate polymerized HbS fiber bundles growing within the cell membrane (Movie S3). The black arrow denotes the direction of flow. Wall shear stress, ~0.05 Pa. FN-coated microchannel wall. (Scale bar: 5 μm.) Area of FOV, ~450 μm^2. (*B*) Simulation results: Adhesion dynamics of an SME at $t = 0$, 15, 65, and 130 s (Movie S4). Wall shear stress, ~0.04 Pa. The green dots in the background matrix represent an array of ligands that simulate a FN-coated adhesion surface, and the dotted circles correspond to effective adhesion binding sites between cell receptors and surface ligands. Initially, the cell has only one adhesion site (white dotted circle); then additional adhesion sites are formed over time (colored dotted circles). (*C*) Number of adhesion sites per cell as a function of time. Instantaneous number of adhesion bond formation (black column) and bond dissociation (red column). *Inset* shows a diagram of the adhesion interaction between the cell and coated surface, where the blue lines represent the adhesion binding sites.

iii) Irregular membrane contour line: The adherent cell's membrane appears more irregular and wavy after 2 min of polymerization than it was at the onset of attachment. The latter is evident at the cell contour from the formation of small menisci, which could also suggest more adhesion sites at the periphery. This can also be indicative of membrane-bound HbS polymerization and simultaneous adhesion on the surface (30). The hypoxic shape is highly irregular, suggesting that there are multiple polymer fibers emerging from the cell that stretch the cell in different directions. These peripheral adhesion sites tend to be strong as they preserve adhesive contact even after reoxygenation (*SI Appendix*, Fig. S7).

Fig. 2*B* shows that under shear flow the SME first undergoes a revolving motion around the adhesion site, which serves as an axis of rotation. This is followed by the formation and dissociation of adhesion binding sites between the cell membrane and the ligands on the wall (colored dotted circles in Fig. 2*B*). The total number of adhesion binding sites depends on the cell wall contact area and the bond reaction rate (k^0_{on}), which may vary in time (*SI Appendix*, *Simulation Model and Method*). For instance, for identical reaction rates, cells of high deformability exhibit large cell wall contact area, hence creating a greater number of adhesion binding sites with time, as shown in Fig. 2*C* (22). We note that an adhesion site corresponds to a bundle of bonds, which can break or form dynamically in the stochastic adhesive dynamics models. Following our previous computational studies (17, 19), the ligands are uniformly distributed on the substrate as a square lattice with lattice length of 1 μm. The cell wall receptor and ligand densities in simulations may be different from those in experiments and correspond to effective cell-to-wall adhesive interactions. However, the intrinsic variability and the stochastic nature of the adhesion process does not alter any of the observations and conclusions of this work.

Regarding the hypoxia shape of the RBCs, it is computationally prohibitive to model polymerization at the molecular level in shear flow. Hence, we directly model the distortion of RBCs induced by the HbS polymers by applying "effective surface tension" on the cell membrane to transform an oxygenated normal (AA) discocyte-shaped RBC into a shape that matches (to a degree possible) the experimental observations (see ref. 22 for details).

In hypoxia alone, the area of adhesive contact varies significantly among cells with different polymerization kinetics. Hence, the combined hypoxia and subsequent normoxia cell adherence images (*SI Appendix*, Fig. S2) may reveal the patient's susceptibility to adhesion via RBC morphological shape change. To this end, we classify adherent SMEs under hypoxia into two categories according to their shape changes compared with their reference shapes under normoxia: (*i*) class I SMEs (SME1s), which exhibit significant morphological shape change under hypoxia, such as Fig. 1, g and h (green dotted circles); and (*ii*) class II mature sickle cells (SME2s), which largely maintain their normoxia shape even under hypoxia (i.e., minimal morphological change) even with irregular surface contour, as shown in Fig. 1, i and f (yellow dotted circles) (*SI Appendix*, *Adherent Sickle Cells*).

On the basis of cell density fractionation results (31) and adherent cell statistics, we note that SME1s are prevalent in the low cell density fractions (~50% of the total cells) (*SI Appendix*, *Adherent Sickle Cells*). SME1s are also cells of high average deformability as measured previously via membrane fluctuations for patients III and IV (31). In contrast, SME2s largely maintain their normoxia shape and consist of ~25% of the total adherent cells in the highest cell density fraction, which is suggestive of less deformability than the adherent SME1s (*SI Appendix*, Fig. S3*C*).

On the basis of the foregoing observations, SME1s may be considered cells of low density and high deformability that are more likely to develop multiple adhesion sites while adherent under hypoxia compared with SME2s and ISCs. They are also more susceptible to adhesion as shown in Fig. 2*C*, consistent with existing evidence (7, 10). These considerations reveal that an assay offering statistics of the most adherent RBCs (i.e., SME1 subpopulation) under hypoxia with respect to the other cell populations could lead to potential correlations with SCD patients' pain crises (*SI Appendix*, Fig. S3*B*).

Adherence of ISCs Under Hypoxia. Sickle cell blood samples contain a subpopulation of abnormally dense cells compared with more uniformly distributed healthy RBCs. Among patients, the dense cell fraction varies greatly in size, from 5 to more than 50% of the total cell population. ISCs are an important constituent of the subpopulation of the abnormally dense cells, and are dehydrated cells with elevated mean cell hemoglobin concentration (2, 32). However, the propensity of ISCs for adhesion to endothelium is less than that of other dense RBCs (3, 33).

Our results show that ISCs adhere relatively rarely (less than 4% of the total adherent cells; *SI Appendix*, Fig. S3*B*) on the FN-coated microchannel wall. In addition, computational simulations reveal that the ISC area involved in adhesive contact remains constant. Furthermore, in contrast to the SMEs (Fig. 2) the ISCs exhibit a relatively low propensity to develop multiple adhesion sites while adherent, as shown in Fig. 3.

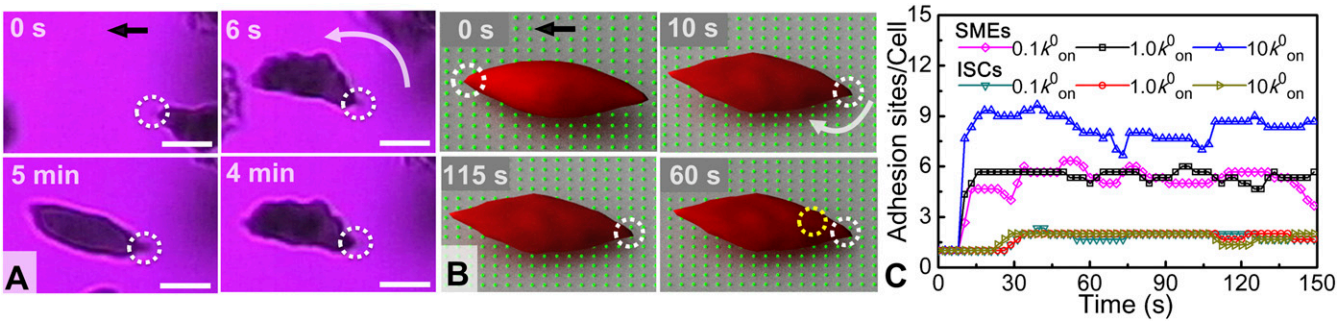

Fig. 3. ISC adhesive dynamics. (*A*) Experiment: successive snapshots of the ISC adherence (cell m, Fig. 1). ($t = 0$) Onset of cell adhesion on the surface, with the adhesion site marked within a white dotted circle in all cases. ($t = 6$ s) The cell flips around the adhesion site to align with the flow direction (Movie S8). (6 s < t < 4 min) The cell exhibits an oscillatory motion due to shear flow. ($t = 5$ min) Reoxygenation: the cell recovers its normoxia shape and maintains its surface adhesion site even after reoxygenation (without detachment). Wall shear stress, ~0.05 Pa. The black arrow denotes the flow direction. (Scale bars: 5 μm.) Area of FOV, ~255 μm^2. (*B*) Simulation: quantitative characterization of the ISC adhesion dynamics with snapshots at $t = 0$, 10, 60, and 115 s (Movie S9). The dotted circles indicate receptor/ligand binding sites. (*C*) Average number of adhesion sites/cell as a function of time, from the simulation, for SMEs and ISCs at different bond formation rates, where k^0_{on} is an equilibrium rate defined in *SI Appendix*, Eq. **S1**.

Fig. 3 shows the evolution of the adhesion dynamics of ISCs under hypoxia and shear flow. The initial attachment site of an ISC is depicted within the white circle in all snapshots. The cell initially adheres to the FN surface following its transformation into hypoxia shape; it subsequently rotates around the attachment point to align with the flow direction. In response to continuous shear flow, the cell exhibits an oscillatory motion around the initial adhesion site for more than 4 min. Following reoxygenation, the cell recovers its normoxia shape and remains attached to the surface at the initial adhesion site (Movie S8). To further investigate the adhesion dynamics of ISCs, we conducted companion simulations for ISCs with an adhesion potential and all other relevant input parameters similar to those employed for SMEs (*SI Appendix*, *Simulation Model and Method*) (22).

As shown in Fig. 3*B*, stochastic bond formation and dissociation occur after the cell rotates around the firm adhesion site. The number of total adhesion sites for ISCs (which are in the range of 1–2) is less than those for SMEs with identical reaction rate (k^0_{on}), due to the lower cell wall contact area caused by low ISC deformability. Through parametric studies for the ISCs, we observed that the total number of adhesion binding sites does not depend strongly on k^0_{on} (Fig. 3*C*). In contrast, SMEs show a significant increase in the number of adhesion binding sites with higher k^0_{on} values (Fig. 3*C*). This result is consistent with prior simulation findings showing that, compared with SMEs, ISCs yield a smaller cell wall contact area, leading to a lower probability to develop adhesion binding sites and thus weaker adhesion (22). Furthermore, in *SI Appendix*, Fig. S4 (*SI Appendix*, *Simulation Model and Method*), we extended our computational sensitivity studies to explore the shape effect of SMEs with respect to the adhesion binding sites. We modeled SMEs of granular, discoid, and elongated shapes, which have comparable cell wall contact areas, and set different values of the bond reaction rate (0.1–10 k^0_{on}). We found that the number of adhesion binding sites is not so sensitive to the SME shapes for the same k^0_{on} value. These findings, therefore, suggest that the probability of cell adhesion is directly correlated with the cell type (which classifies cell maturity) rather than with the number of adhesion binding sites.

Adhesion Favors Polymerization in Sickle RBCs. Adhesion prolongs the residence time of sickle RBCs in hypoxia before the morphological sickling event, while sickling occurs instantaneously. Fig. 4 shows snapshots of the intermediate or transitional stages of adhesion dynamics of SMEs under hypoxia. The cells attach to the wall having their normoxia shape even though they have been exposed to hypoxia for ~2 min before attachment. The cells retain their normoxia shape while adherent for about 6 min (under hypoxia and shear flow). During this time, localized area darkening is taken to be indicative of the accumulation of Hb polymer within the cell. The cells finally attain their hypoxia shape, which also reveals underlying adhesion sites. This is accompanied by the formation of a polymerization front (*SI Appendix*, Fig. S5).

The transitional stages described in Fig. 4 for SMEs from the onset of sickling are similar to those of SME1s described previously. The key difference is the significantly increased delay time in morphological sickling events. However, how RBC membrane influences polymerization is not fully understood. RBC morphological sickling depends strongly on the Hb concentration, the proportion of Hb that is irreversibly associated with the membrane and the amounts of free heme (34, 35). Our observations suggest that, even before the morphological sickling event, sickle RBCs are still prone to adhesion and that, while adherent for long periods, they can experience morphological sickling. The latter trend suggests that adhesion indirectly promotes polymerization by increasing the residence time of the adherent RBCs and strongly points to the bidirectional coupling between adhesion and polymerization.

Polymerization Favors Adhesion in SRs. We isolated SRs to further explore their unique polymerization kinetics (*SI Appendix*, *Adherent Sickle Cells*). The adhesive dynamics and simultaneous polymerization of an SR are presented in Fig. 5 and *SI Appendix*,

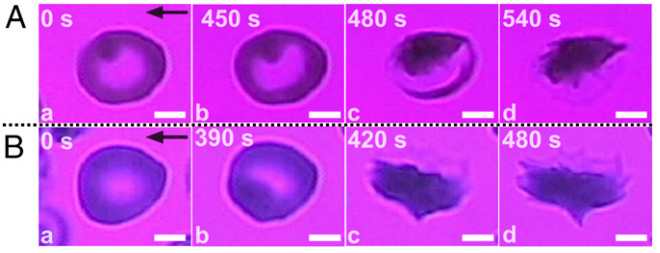

Fig. 4. Adhesion stimulates polymerization in SMEs under hypoxia through a variety of transition mechanisms and residence times. (*A*) ($t = 0$) Initial cell attachment on the FN-coated wall surface. Localized area darkening is interpreted as regional accumulation of Hb within the cell. ($t = 450$ s) Cell morphology at the onset of transition; slight intracellular Hb content reorganization is evident. ($t = 480$ s) Bulk polymerized part of the cell is revealed. ($t = 540$ s) The cell attains its hypoxia shape (cell d in Movie S1). Wall shear stress, ~0.05 Pa. Area of FOV, ~102 μm^2. (*B*) ($t = 0$) Initial cell attachment on the FN-coated wall surface. ($t = 390$ s) Cell morphology at the onset of transition. ($t = 420$ s) Apparent snap-through transition. ($t = 480$ s) The cell attains its hypoxia shape, and underlying adhesion sites are revealed (*SI Appendix*, Fig. S5). Wall shear stress, ~0.08 Pa. Area of FOV, ~120 μm^2. Black arrows denote flow direction. (Scale bars: 2.5 μm.)

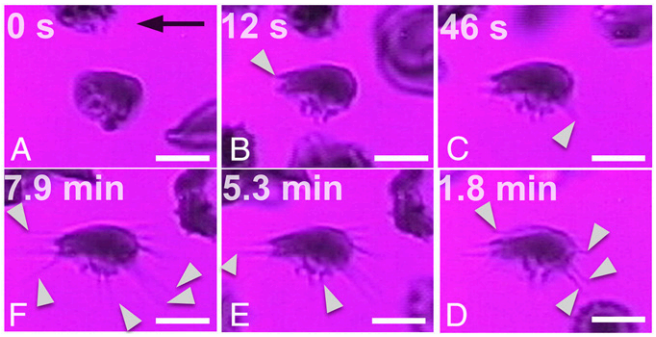

Fig. 5. Simultaneous adhesion and polymerization in SRs under hypoxia and shear flow (cell b in Fig. 1), observed at different time points (*A*–*F*). (t = 0) The cell adheres on the surface. (9 s < t < 1.8 min) Gradual protrusion of polymerized HbS fibers (white pointers) and apparent increase of the overall projected bulk cell surface area. (54 s < t < 7.9 min) Fiber bundles continue to grow outward of the bulk of the cell (white pointers) (Movie S5). The black arrow denotes the flow direction. Wall shear stress, ~0.05 Pa. FN-coated microchannel wall. (Scale bar: 5 μm.) Area of FOV, ~290 μm^2.

Fig. S6 for experimental conditions identical to those described previously, that is, conditions involving cell attachment to a FN-coated microchannel wall under steady-state hypoxia and shear flow. The main observations are as follows: (*i*) Multiple HbS polymer fibers grow from the cell bulk irrespectively of the flow direction: HbS fiber projections attach onto the surface while gradually (12 s < t < 7.9 min) growing outward of the cell in random directions (white pointers in Fig. 5). (*ii*) Significant increase of the projected cell surface area: Following initial adhesion and concurrently with polymerization (~8 min), the cell stretches in different directions on the surface, driven by the outward growth of fibers. The apparent increase of the cell's contact area between Fig. 5 *A* and *F* is estimated to be more than twice that of the initial projected surface area (*SI Appendix*, Fig. S6*A*).

Subsequent reoxygenation of SRs—while still adherent to the surface—reveals residual posthypoxia adhesion sites. Specifically, Fig. 6 shows adherent SR1s (least mature marrow reticulocytes; Fig. 5 and *SI Appendix*, Fig. S6) and an SR2 (more mature marrow reticulocyte with asymmetric morphology; *SI Appendix*, Fig. S7 and Movie S12) during a hypoxia-to-reoxygenation cycle (*SI Appendix*, *Adherent Sickle Cells*).

Time-lapse images are shown in Fig. 6 for SRs adherent under hypoxia for 7–9 min, following which they were reoxygenated. During this hypoxia-to-reoxygenation cycle, the following observations were made: (*i*) The polymerized HbS fibers that protrude from the initial cell boundary retract into the cell upon reoxygenation (Fig. 6, *II*). This result provides clear indication that the cells did not experience lysis and that the lipid bilayer also stretches following the contact line of the fiber projections (Fig. 6, *I*). (*ii*) Residual posthypoxia adhesion sites are evident in SR1 (dotted green circles in Fig. 6 *A*, *II*). Residual posthypoxia adhesion sites are also very common in the SME1 population (*SI Appendix*, Fig. S7).

Although the membrane of the SR1 contains folds (23), it is a continuous structure. Our observations suggest that the SR1 membrane can be stretched to allow HbS polymer fibers to protrude outward from initial cell boundary. Furthermore, all adherent cells under hypoxia remain adherent to the surface even after subsequent reoxygenation.

Discussion and Concluding Remarks

Systemic vasoocclusive pain crisis is the predominant pathophysiology in SCD patients, caused by HbS polymerization that leads to abnormal sickle RBC rheology and premature hemolysis (36). Hemolytic anemia is a common occurrence in SCD patients due to the presence of mechanically fragile RBCs that are prone to lysis. The resulting anemia prompts the bone marrow to compensate and increase red cell production. As a result, significantly elevated levels of SRs have been reported for patients with different types of anemia (23, 37). Elevated numbers of reticulocytes have also been reported (37) in peripheral blood due to increased chronic erythropoietic stress. As indicated in *SI Appendix*, Fig. S3, we also observe a relatively large proportion of adherent reticulocytes in all patient samples tested (more than 10% of the total adherent population in some cases).

In addition, HbS fiber projections, expressed in SRs and SME1s, could lead to points of adhesion. High-resolution microscopy studies (9, 38) also reveal that neutrophils and platelets form similar protrusions. The termini of these "slings" serve as points of adhesion involving P-selectin.

In SCD patients, up to 25% of SRs express the $\alpha_4\beta_1$-integrin complex that is broadly distributed within the cell membrane, and this complex mediates both cell–cell and cell–matrix interactions. By contrast, the overall concentration of $\alpha_4\beta_1$-expressing healthy erythrocytes is less than 5%. In particular, the expression of VCAM-1 on vascular endothelium provides a ligand for binding of $\alpha_4\beta_1$-integrin–expressing SRs that mediate cell binding to cytokine-activated endothelium (39, 40). Moreover, binding of SRs in $\alpha_4\beta_1$ activated by phorbol ester or chemokine IL-8 to endothelial cell-associated FN has also been reported (41). Last, hypoxia up-regulates both the expression of VCAM-1 and ICAM-1 in endothelial cells themselves, and the least dense sickle cells containing $CD36^+$ and VLA-4^+ reticulocytes show significantly increased binding compared with the normoxia controls, via the adhesive receptor combination VCAM-1–VLA-4 (13). Therefore, it is likely that HbS projections adherent to FN involve the $\alpha_4\beta_1$-integrin pathway.

Our results also suggest that the cell membrane structure of SRs may play an additional role in mediating adhesion, in that SRs have more membrane available to be able to form projections. Moreover, any dissociations between the lipid bilayer and cytoskeleton (vertical interaction), or within the cytoskeleton (horizontal interaction) or both, could play a role in membrane stretching and in influencing how the polymerized HbS fiber bundles grow outward of the initial cell boundary (42).

One notable distinction between SRs and any other cell category examined in this work is that, in SRs, the HbS projections

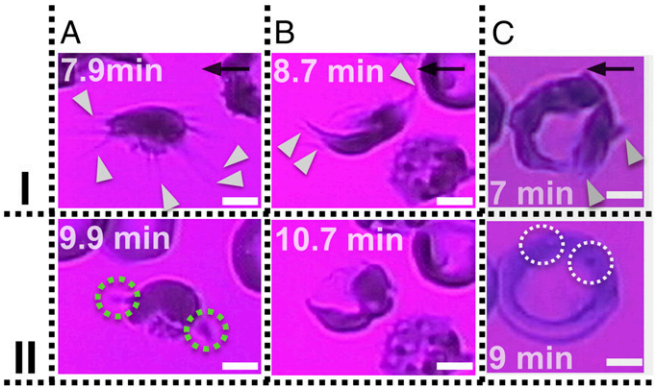

Fig. 6. Reoxygenation in SR1s (*A* and *B*) and SR2 (*C*) reticulocytes; polymerized HbS fiber bundles retract after reoxygenation. (*I*) Adherent cells under hypoxia for up to 9 min; onset of reoxygenation (*II*) after 2 min of reoxygenation. (*A*) SR1 of Fig. 5: (t = 9.9 min) The polymerized HbS fibers retract back to the cell bulk. The green dotted circles indicate residual adhesion sites (Movie S10). (*B*) SR1 of *SI Appendix*, Fig. S6: (t = 10.7 min) The polymerized HbS fibers retract back to the cell bulk (Movie S11). (*C*) SR2 of Movie S12: HbS polymer projections (white pointers) have grown outside of the cell's ring. (t = 9 min) Reoxygenation shows that the SR2 recovers the "deep-dish" morphology. The white dotted circles show the visible granules within the refractile ring. Wall shear stress, ~0.05 Pa. The black arrows denote flow direction. (Scale bars: 2.5 μm.)

grow and protrude outward of the initial membrane/cell boundary. This leads to a significant increase of the cell-to-wall contact area, and hence the probability for adhesion increases, as indicated by our simulations.

The energy to dissociate lipid bilayer from cytoskeleton of SRs can be four times smaller than SMEs (43), suggesting that the interactions between the cytoskeleton and the lipid bilayer are weaker. In SMEs, however, the stronger lipid bilayer–cytoskeleton cohesion is associated with less pronounced fiber growth within the cell membrane. The latter is consistent with our observations, which is a very distinct attribute of membrane remodeling during maturation.

In conclusion, we have shown that hypoxia significantly enhances the sickle RBC cytoadherence compared with normoxia controls under low shear stress (typically smaller than 0.1 Pa). Our results reveal cell-level consequences of simultaneous polymerization, cytoadherence, and cell maturation. We find that hypoxia enhances the adhesion of SMEs and SRs to surfaces. In particular, SR1s grow HbS projections, uniquely stretching the cell outward while simultaneously adhering onto the surface. The propensity for adhesion is seen to rank with sickle cell maturation stage as follows: SRs → SME1s → SME2s → ISCs. Our computational simulations qualitatively confirm these observations and trends, and they also quantify the number of adhesion binding sites that change with time. Furthermore, our simulations show that deformable SMEs are sensitive to increases in the binding reaction rate, in contrast to more rigid ISCs. A key finding of our work is that adhesion stimulates polymerization under long-term hypoxia, reflecting the bidirectional synergistic coupling between adhesion and polymerization.

Methods

Blood Specimens. Blood samples were drawn from homozygous SS SCD patients at the University of Pittsburgh (Pittsburgh) (University of Pittsburgh IRB protocol PRO08110422) and the Massachusetts General Hospital (Boston) under a protocol of Excess Human Materials approved by the Partners Healthcare IRB with a waiver of consent. More details are in *SI Appendix, Blood Specimens*.

Device Fabrication and Experimental Setup. The microfluidic devices were fabricated using FN-functionalized polydimethylsiloxane. More details are in *SI Appendix*.

Simulation Model and Method. We simulated the sickle RBCs using a multiscale RBC model based on DPD. More details are in *SI Appendix, Simulation Model and Method*.

ACKNOWLEDGMENTS. We thank Prof. John Higgins, Jude Jonassaint, Nancy Petro, and Yingze Zhang for providing sickle blood samples and Profs. Peter Vekilov and Pierre Buffet for helpful discussions. G.E.K. acknowledges support from the computing resources at Argonne National Laboratory/Oakridge. S.S. acknowledges support from Nanyang Technological University through the Distinguished University Professorship. We acknowledge support from NIH Grants U01HL114476 and R01HL121386.

1. Hebbel RP (2008) Adhesion of sickle red cells to endothelium: Myths and future directions. *Transfus Clin Biol* 15:14–18.
2. Hebbel RP (1991) Beyond hemoglobin polymerization: The red blood cell membrane and sickle disease pathophysiology. *Blood* 77:214–237.
3. Hebbel RP, et al. (1980) Abnormal adherence of sickle erythrocytes to cultured vascular endothelium: Possible mechanism for microvascular occlusion in sickle cell disease. *J Clin Invest* 65:154–160.
4. Kaul DK, Fabry ME, Nagel RL (1989) Microvascular sites and characteristics of sickle cell adhesion to vascular endothelium in shear flow conditions: Pathophysiological implications. *Proc Natl Acad Sci USA* 86:3356–3360.
5. Hebbel RP, Boogaerts MAB, Eaton JW, Steinberg MH (1980) Erythrocyte adherence to endothelium in sickle-cell anemia. A possible determinant of disease severity. *N Engl J Med* 302:992–995.
6. Kaul DK, Chen D, Zhan J (1994) Adhesion of sickle cells to vascular endothelium is critically dependent on changes in density and shape of the cells. *Blood* 83:3006–3017.
7. Kaul DK, Finnegan E, Barabino GA (2009) Sickle red cell–endothelium interactions. *Microcirculation* 16:97–111.
8. Fabry ME, et al. (1992) Demonstration of endothelial adhesion of sickle cells in vivo: A distinct role for deformable sickle cell discocytes. *Blood* 79:1602–1611.
9. Sundd P, et al. (2012) "Slings" enable neutrophil rolling at high shear. *Nature* 488: 399–403.
10. Manwani D, Frenette PS (2013) Vaso-occlusion in sickle cell disease: Pathophysiology and novel targeted therapies. *Blood* 122:3892–3898.
11. Zhang D, Xu C, Manwani D, Frenette PS (2016) Neutrophils, platelets, and inflammatory pathways at the nexus of sickle cell disease pathophysiology. *Blood* 127:801–809.
12. Montes RAO, Eckman JR, Hsu LL, Wick TM (2002) Sickle erythrocyte adherence to endothelium at low shear: Role of shear stress in propagation of vaso-occlusion. *Am J Hematol* 70:216–227.
13. Setty BN, Stuart MJ (1996) Vascular cell adhesion molecule-1 is involved in mediating hypoxia-induced sickle red blood cell adherence to endothelium: Potential role in sickle cell disease. *Blood* 88:2311–2320.
14. Du E, Diez-Silva M, Kato GJ, Dao M, Suresh S (2015) Kinetics of sickle cell biorheology and implications for painful vasoocclusive crisis. *Proc Natl Acad Sci USA* 112: 1422–1427.
15. Joneckis CC, Ackley RL, Orringer EP, Wayner EA, Parise LV (1993) Integrin alpha 4 beta 1 and glycoprotein IV (CD36) are expressed on circulating reticulocytes in sickle cell anemia. *Blood* 82:3548–3555.
16. Stone PCW, Stuart J, Nash GB (1996) Effects of density and of dehydration of sickle cells on their adhesion to cultured endothelial cells. *Am J Hematol* 52:135–143.
17. Bell GI (1978) Models for the specific adhesion of cells to cells. *Science* 200:618–627.
18. Hammer DA, Apte SM (1992) Simulation of cell rolling and adhesion on surfaces in shear flow: General results and analysis of selectin-mediated neutrophil adhesion. *Biophys J* 63:35–57.
19. McEver RP, Zhu C (2010) Rolling cell adhesion. *Annu Rev Cell Dev Biol* 26:363–396.
20. Fedosov DA, Caswell B, Karniadakis GE (2011) Wall shear stress-based model for adhesive dynamics of red blood cells in malaria. *Biophys J* 100:2084–2093.
21. King MR, Hammer DA (2001) Multiparticle adhesive dynamics: Hydrodynamic recruitment of rolling leukocytes. *Proc Natl Acad Sci USA* 98:14919–14924.
22. Lei H, Karniadakis GE (2013) Probing vasoocclusion phenomena in sickle cell anemia via mesoscopic simulations. *Proc Natl Acad Sci USA* 110:11326–11330.
23. Chasis JA, Prenant M, Leung A, Mohandas N (1989) Membrane assembly and remodeling during reticulocyte maturation. *Blood* 74:1112–1120.
24. Coulombel L, Tchernia G, Mohandas N (1979) Human reticulocyte maturation and its relevance to erythropoietic stress. *J Lab Clin Med* 94:467–474.
25. Kaul DK, Fabry ME, Windisch P, Baez S, Nagel RL (1983) Erythrocytes in sickle cell anemia are heterogeneous in their rheological and hemodynamic characteristics. *J Clin Invest* 72:22–31.
26. Mel HC, Prenant M, Mohandas N (1977) Reticulocyte motility and form: Studies on maturation and classification. *Blood* 49:1001–1009.
27. Mohandas N, Evans E (1985) Sickle erythrocyte adherence to vascular endothelium. Morphologic correlates and the requirement for divalent cations and collagen-binding plasma proteins. *J Clin Invest* 76:1605–1612.
28. Xu M, et al. (2017) A deep convolutional neural network for classification of red blood cells in sickle cell anemia. *PLoS Comput Biol* 13:e1005746.
29. Hebbel RP (1997) Perspectives series: Cell adhesion in vascular biology. Adhesive interactions of sickle erythrocytes with endothelium. *J Clin Invest* 99:2561–2564.
30. Eisinger J, Flores J, Bookchin RM (1984) The cytosol-membrane interface of normal and sickle erythrocytes. Effect of hemoglobin deoxygenation and sickling. *J Biol Chem* 259:7169–7177.
31. Hosseini P, et al. (2016) Cellular normoxic biophysical markers of hydroxyurea treatment in sickle cell disease. *Proc Natl Acad Sci USA* 113:9527–9532.
32. Billett HH, Kim K, Fabry ME, Nagel RL (1986) The percentage of dense red cells does not predict incidence of sickle cell painful crisis. *Blood* 68:301–303.
33. Mohandas N, Evans E (1984) Adherence of sickle erythrocytes to vascular endothelial cells: Requirement for both cell membrane changes and plasma factors. *Blood* 64: 282–287.
34. Eaton WA, Hofrichter J (1987) Hemoglobin S gelation and sickle cell disease. *Blood* 70: 1245–1266.
35. Galkin O, Vekilov PG (2004) Mechanisms of homogeneous nucleation of polymers of sickle cell anemia hemoglobin in deoxy state. *J Mol Biol* 336:43–59.
36. Eaton WA, Bunn HF (2017) Treating sickle cell disease by targeting HbS polymerization. *Blood* 129:2719–2726.
37. Perrotta AL, Finch CA (1972) The polychromatophilic erythrocyte. *Am J Clin Pathol* 57: 471–477.
38. Bennewitz MF, et al. (2017) Lung vaso-occlusion in sickle cell disease mediated by arteriolar neutrophil-platelet microemboli. *JCI Insight* 2:e89761.
39. Gee BE, Platt OS (1995) Sickle reticulocytes adhere to VCAM-1. *Blood* 85:268–274.
40. Swerlick RA, Eckman JR, Kumar A, Jeitler M, Wick TM (1993) Alpha 4 beta 1-integrin expression on sickle reticulocytes: Vascular cell adhesion molecule-1-dependent binding to endothelium. *Blood* 82:1891–1899.
41. Kumar A, Eckmam JR, Swerlick RA, Wick TM (1996) Phorbol ester stimulation increases sickle erythrocyte adherence to endothelium: A novel pathway involving alpha 4 beta 1 integrin receptors on sickle reticulocytes and fibronectin. *Blood* 88:4348–4358.
42. Li H, et al. (2018) Cytoskeleton remodeling induces membrane stiffness and stability changes of maturing reticulocytes. *Biophys J* 114:2014–2023.
43. Hochmuth RM, Waugh RE (1987) Erythrocyte membrane elasticity and viscosity. *Annu Rev Physiol* 49:209–219.